Schistosoma mansoni cercariae swim efficiently by exploiting an elastohydrodynamic coupling

Deepak Krishnamurthy[1], Georgios Katsikis[1], Arjun Bhargava[2] and Manu Prakash[3]★

The motility of many parasites is critical for infecting their host, as exemplified in the transmission cycle of the parasite *Schistosoma mansoni*[1]. In its human infectious stage, sub-millimetre-scale forms of the parasite known as cercariae swim in freshwater and infect humans by penetrating the skin[1,2]. This infection causes schistosomiasis, a disease comparable to malaria in global socio-economic impact[3,4]. Given that cercariae do not feed and hence have a lifetime of around 12 hours[5,6], efficient motility is crucial for schistosomiasis transmission. Despite this, a first-principles understanding of how cercariae swim is lacking. Combining biological experiments, a novel theoretical model and its robotic realization, we show that cercariae use their forked tail to swim against gravity using a novel swimming gait, described here as a 'T-swimmer gait'. During this gait, cercariae beat their tail periodically while maintaining an increased flexibility near their posterior and anterior ends. This flexibility allows an interaction between fluid drag and bending resistance—an elastohydrodynamic coupling, to naturally break time-reversal symmetry and enable locomotion at small length scales[7]. Finally, we find that cercariae maintain this flexibility at an optimal regime for efficient swimming. We anticipate that our work sets the ground for linking the swimming of cercariae to disease transmission, and could potentially enable explorations of novel strategies for schistosomiasis control and prevention.

In their natural habitat of rivers and ponds, *S. mansoni* cercariae are released from intermediate snail hosts and aggregate below the water surface to increase their chances of finding a human host[8,9] (Fig. 1a). The cercariae are around 500 μm long and consist of an anterior body, a slender tail and a posterior bifurcation of the tail called the 'furca', henceforth termed the fork (Fig. 1b)[10,11]. Being negatively buoyant, they need to swim against gravity to stay near the water surface, which they accomplish by using their fork (Fig. 1b (i))[10,11]. The fork is an uncommon appendage, not found in any well-studied swimming microorganisms such as bacteria[12], or ciliates[13,14]. Also, unlike the aforementioned microorganisms, cercariae do not feed[5,6]. Hence their swimming efficiency is an important determinant of their ability to survive longer to find and infect humans. For such an important human parasite, while a body of work has focused on the behavioural[1,2] and qualitative aspects[10,15] of cercarial motility, the swimming mechanics of cercariae remains unknown.

To mimic the natural habitat of cercariae we conducted laboratory experiments with multiple freely swimming specimens in a 4 cm × 1 cm × 1.4 mm chamber which is much larger than their own size (≈500 μm). We observed that cercariae display an intermittent swimming behaviour consisting of three modes[10,11] (Fig. 1b and Supplementary Movie 1 and 2): A tail-first mode in which they swim up against gravity with their

fork fully extended (Fig. 1b (i)), a free-sinking mode on account of being negatively buoyant where the fork is partially extended (Fig. 1b (ii)), and a body-first mode which is used to approach towards the skin, where the fork is folded back (Fig. 1b (iii)). We analysed trajectories ($n = 2{,}774$ segments; Supplementary Methods) of individual cercariae and obtained the relative time durations spent in each mode. We found that cercariae spend a majority of their time in the free-sinking mode (83% of the total time) with a mean sinking speed $\langle V_{\text{sinking}} \rangle = 0.1\,\text{mm s}^{-1}$, followed by the tail-first swimming mode (17%) with $\langle V_{\text{tail-first}} \rangle = 0.7\,\text{mm s}^{-1}$. The body-first mode is often triggered by chemical cues[16–18] which are absent in our current experiments, leading to very few observed trajectories (<0.1%). Despite the fact that cercariae spend longer periods of time freely sinking, we expect that most of the energy consumption occurs during the tail-first mode[5], since this involves active swimming. Thus, the swimming efficiency of the tail-first mode directly affects the ability of cercariae to aggregate near the water surface to increase chances of encountering a human host. Also, given that the swimming gait of cercariae in the tail-first mode is distinct from that of well-studied microorganisms[14], it is of fundamental interest to understand its mechanics.

To study the tail-first swimming mode we conducted high-speed imaging experiments (Supplementary Methods) on individual cercariae. We observed that cercariae swim using a periodic gait, wherein they beat their tail from side to side with a frequency f in the range 15–20 Hz (Fig. 2a and Supplementary Movie 3). In addition to this periodic beating of the tail, cercariae also undergo a much slower rotation about an axis parallel to their swimming direction, causing the plane in which the tail beats to rotate slowly over time. However, this is much slower (taking ≈840 ms for a complete rotation) than a swimming cycle ($t_{\text{cycle}} = 1/f \approx 50\,\text{ms}$), hence justifying a two-dimensional description of the swimming motion. The origin and role of this slow rotation are beyond the scope of this paper and offer opportunities for future work.

For understanding the hydrodynamics of cercarial swimming and the relative contribution of inertial and viscous forces, we estimated the relevant Reynolds number $\text{Re} = \langle V_{\text{tail-first}} \rangle L / \nu \approx 0.3$, where $L \approx 500\,\mu\text{m}$ is the organism length and $\nu = 10^{-6}\,\text{m}^2\,\text{s}^{-1}$ is the kinematic viscosity of the ambient fluid (water). This $\text{Re} < 1$ indicates the relative dominance of viscous over inertial forces in the swimming. To confirm this we measured the flow field around the organism using particle image velocimetry (PIV) (Supplementary Methods) and observed regions of recirculating fluid (vortices) which remain adjacent to the organism (Fig. 2d,e and Supplementary Movie 4). We have further analysed metrics of the flow surrounding the cercariae (Supplementary Fig. 1) and demonstrated that inertial forces may be neglected in studying cercarial swimming. We therefore studied the hydrodynamics of

[1]Department of Mechanical Engineering, Stanford University, Stanford, California 94305, USA. [2]Department of Applied Physics, Stanford, California 94305, USA. [3]Department of Bioengineering, Stanford University, Stanford, California 94305, USA. *e-mail: manup@stanford.edu
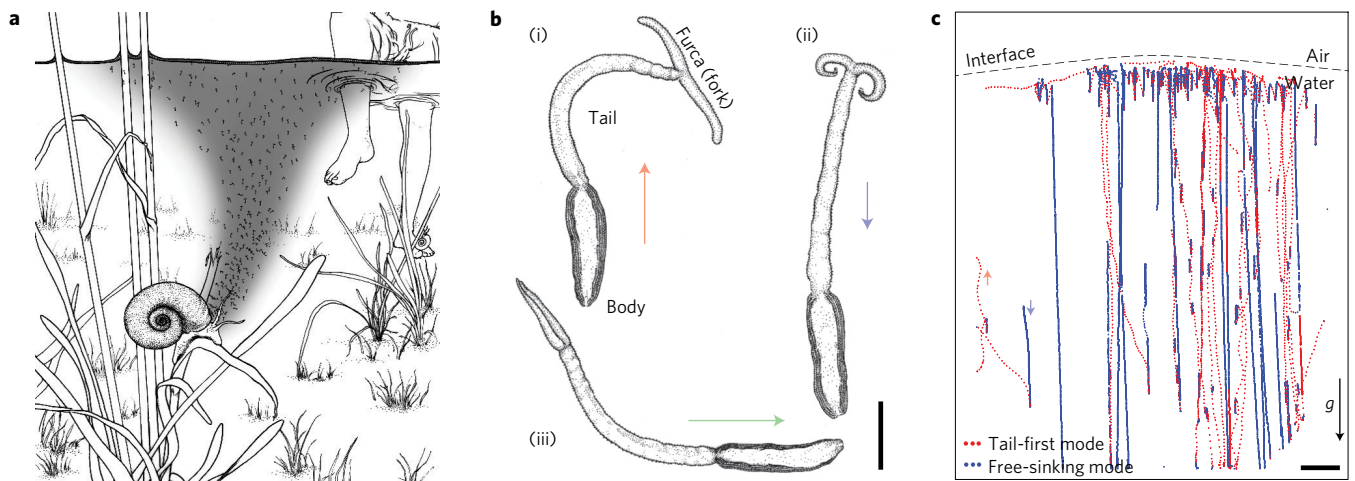
Figure 1 | Macroscale swimming behaviour of *Schistosoma mansoni* cercariae. a, Artistic rendering (not to scale) of a typical transmission site where cercariae (immature, human infectious stage of the parasites) emerge into freshwater from snails and aggregate near the water surface[8]. **b**, Artistic rendering of the three distinct modes displayed by cercariae in their intermittent swimming behaviour (Supplementary Video 1) termed (i) tail-first mode, (ii) free-sinking mode and (iii) body-first mode. Arrows indicate the direction of motion. Scale bar, 100 μm. **c**, Computationally tracked snapshot of cercariae swimming in a vertical chamber (Supplementary Methods) showing tail-first swimming (red) and sinking (blue) trajectories for 10 min (Supplementary Movie 2). The resulting tracks of organisms have a strikingly columnar nature (Supplementary Movie 2) with very little drift in the horizontal direction. This is due to the fact that cercariae are bottom-heavy swimmers (Supplementary Fig. 2) and undergo a gravitational realignment such that their longitudinal axis is aligned with the vertical with the body pointing down. Scale bar, 1 mm.

cercarial swimming using purely viscous or Stokes flow theories which correspond to the limit Re = 0 (ref. 19).

To achieve locomotion, cercariae, like any swimmer dominated by viscosity, must change their shape in a manner that breaks time-reversal symmetry[7,13]. Using image analysis we extracted the dynamic shape of the organism (Fig. 2a) and observed that their periodic gait consists of successive power and recovery strokes that break time-reversal symmetry. During a power stroke, the tail bends from a straightened state to its maximally curved state, while the fork sweeps out an arc, moving almost perpendicular to its longitudinal axis (sequence 1 → 2 in Fig. 2a,c,d,f and Supplementary Movie 5). The fork's motion is directed towards the body of the organism, generating a thrust force that pulls the body forward along the mean swimming direction $\hat{s}$ (sequence 1 → 2 in Fig. 2a,c). During a recovery stroke the tail returns to its straightened state and the fork moves parallel to its own longitudinal axis (sequence 2 → 3 in Fig. 2a,c,e,f and Supplementary Movie 5), pushing the body backwards. Owing to the different orientation of the fork, this backward displacement is smaller than that during the power stroke, thus leading to a cumulative displacement of the body along $\hat{s}$. The body of the organism additionally generates thrust by breaking time-reversal symmetry (sequence 1 and 3 in Fig. 2c,f) in a manner similar to conventional Stokesian swimming strategies which involve waving an elastic arm[20].

At low Re the fluid drag on a body is only weakly anisotropic as compared to the same body at high Re. For slender bodies, such as the fork in cercariae (aspect ratio ≈ 20), the drag at low Re is around twice as large when the body moves perpendicular to its longitudinal axis as compared to parallel to this axis[21]. By moving the fork perpendicular and parallel to its axis during the power and recovery strokes, respectively (Supplementary Movie 5), cercariae seem to maximally utilize this weak anisotropy.

The kinematics of the fork and body in relation to the tail, as quantified by the respective joint angles (Fig. 2b), highlight the non-reciprocal nature of the swimming gait which breaks time-reversal symmetry (Fig. 2f). Interestingly, the tail bends symmetrically and does not contribute to the breaking of time-reversal symmetry (right axis of Fig. 2c). Therefore cercarial locomotion crucially depends on the degree of freedom at the

tail–fork and tail–body joints (Fig. 2b). These degrees of freedom appear to be a result of increased local flexibility in the joints due to smooth-muscle-mediated constrictions in the transverse dimension of the organism[10,22].

To further understand the swimming mechanism and exactly how these joint angles evolve over time, we hypothesize the simplest passive control strategy where a balance between elastic bending stiffness and viscous drag forces dictates the exact kinematics of cercarial swimming—an elastohydrodynamic effect, rather than active muscular control. We conjecture that cercariae maintain a fixed local stiffness at these joints using smooth musculature, modifying only the joint stiffness when they change their swimming mode. Our hypotheses are supported by earlier studies, which demonstrate that the striated muscles that are capable of rapid beating are confined to the tail, and not present in the fork[11,23]. To test our hypotheses we developed a theoretical model: a 'T-swimmer', consisting of three, linear, rigid links (Fig. 3a (ii)). The first two links correspond to the fore and aft ends of the body–tail portion in cercariae, and the third link, which is attached transversely at its midpoint, corresponds to the fork (Fig. 3a (i) and (ii)). In our geometry, as a starting point, we neglect the body in cercariae and also the effects of gravity, to make the simplest possible swimming model (Fig. 3a (ii)). As the reader will quickly notice, our 'T-swimmer' is inspired by Purcell's three-link-swimmer[7], often referred to as the simplest low-Reynolds-number swimmer since it requires only two actively actuated joints. In contrast to Purcell's swimmer, in the T-swimmer only a single longitudinal joint is actively actuated (red dot in Fig. 3a (ii)), to model the bending of the tail of cercariae, while the transverse joint is passive and assumed to be a linear torsional spring (blue spiral in Fig. 3a (ii)).

The parameters of the T-swimmer include the lengths of the links (l_1, l_2, l_3) and their transverse dimensions (r_1, r_2, r_3); the actuation amplitude of the active joint A, the driving frequency f and the torsional stiffness of the passive joint Γ_{tf} (Fig. 3a (ii)). We non-dimensionalized the system using the half-length of the organism $l_c = L/2$ and the timescale $t_c = 1/f$. The force and torque scales follow the viscous scaling $F_c = \mu f l_c^2$ and $\tau_c = \mu f l_c^3$, respectively[19]. Therefore the key dynamical parameter of the system is the dimensionless torsional stiffness $\hat{\Gamma}_{tf} = \Gamma_{tf}/(\mu f l_c^3)$.
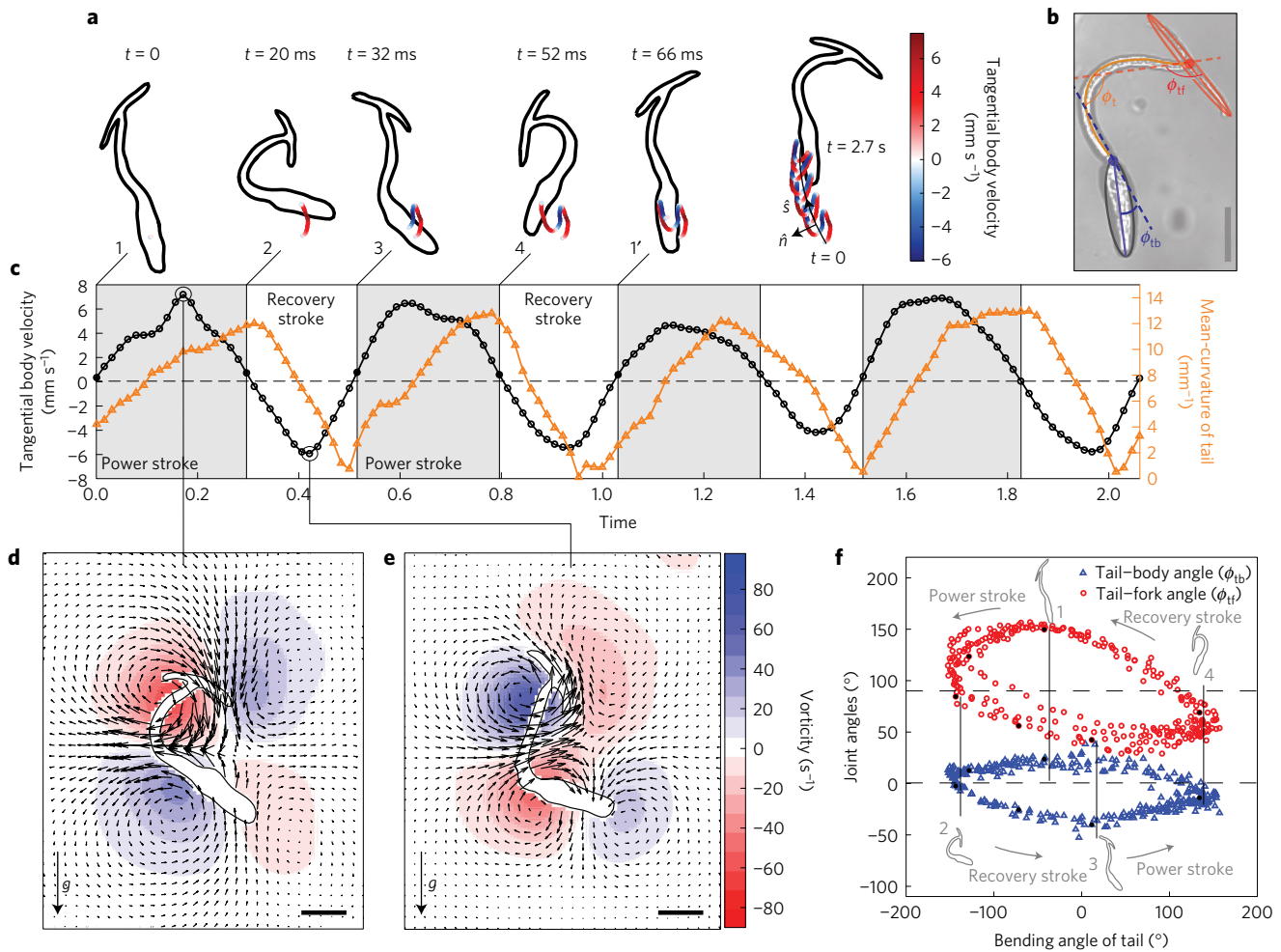
Figure 2 | Shape kinematics of *S. mansoni* cercariae swimming in the tail-first mode. a, Extracted dynamic shapes from high-speed videos of cercariae at different time points during a swimming cycle (Supplementary Methods). The trajectory of the body is colour-coded based on the instantaneous velocity magnitude along the local tangent ($\hat{s}$) to the mean swimming trajectory, shown as a solid black line in the last panel. **b**, Illustration of kinematic parameters: the angle at the tail–body joint ϕ_{tb} shown in blue, the angle at the tail–fork joint ϕ_{tf} shown in red and an effective bending angle of the tail ϕ_t shown in orange. **c**, Time series plot of the tangential body velocity along $\hat{s}$ (left axis) demonstrates forward motion although the mean-curvature of the tail (right axis) is symmetric, seemingly appearing to be a reciprocal stroke. Grey regions ($1 \rightarrow 2, 3 \rightarrow 4$ and so on) correspond to power strokes where the body of the organism has a tangential velocity in the mean swimming direction, while white regions ($2 \rightarrow 3, 4 \rightarrow 1'$ and so on) are recovery strokes where the body moves in the opposite direction. Time is normalized by $1/f$, where $f = 15.6$ Hz is the beat frequency. **d,e**, Snapshots of the transient flow velocity exhibiting reversing stagnation points. Vorticity fields obtained using particle image velocimetry (PIV) during the power stroke and recovery stroke, respectively. The regions of vorticity remain attached to the organism and are not shed (Supplementary Movie 4). **f**, Phase plot of ϕ_{tb} and ϕ_{tf} as a function of ϕ_t clearly shows a finite area, hence revealing the role of tail–fork and tail–body joints in producing a non-reciprocal swimming stroke, required for low-Reynolds-number swimming. Scale bars, 100 μm.

To specify the hydrodynamic forces and torques on the T-swimmer we used local slender-body-theory[21] and solved the resulting equations of motion numerically (Supplementary Section 3.1). Our results show that the T-swimmer swims with the passive joint preceding the active one, kinematically similar to cercariae swimming tail-first (Supplementary Video 6). In contrast, a slight variation of the classic Purcell's swimmer, which has one active and one passive joint, swims in an opposite direction to the T-swimmer, with the active joint preceding the passive one (Supplementary Movie 6 and ref. 24). Our results demonstrate that a simple transition from a longitudinal to a transverse link, either of which are attached via a torsional spring, results in a reversal in swimming direction (Supplementary Movie 6)—a viable strategy for any organism trying to reverse swimming directions from body-first to tail-first.

For validating our theory we also performed scaled-up experiments on a centimetre-scale ($L_{robot} \approx 10$ cm) robot mimicking

our T-swimmer (Fig. 3a (iii)). The robot was immersed in a corn-syrup medium to achieve dynamically similar conditions ($Re_{robot} \approx 0.2$) to swimming cercariae (Supplementary Methods). We found that both the T-swimmer (Fig. 3b) and the robot (Fig. 3c) reproduce the non-reciprocal swimming gait of cercariae, thereby supporting our hypothesis (Fig. 2f). For both the T-swimmer and the robot, we varied $\hat{\Gamma}_{tf}$ and A and found that in the upper and lower limits of joint stiffness ($\hat{\Gamma}_{tf} \gg 1$ and $\hat{\Gamma}_{tf} \ll 1$), the gait becomes reciprocal (Fig. 3b,c) and the swimming speed averaged over > 20 cycles is negligible (Fig. 3d,e,f). This is explained by the fact that for $\hat{\Gamma}_{tf} \gg 1$ the swimmer has a single degree of freedom, since the tail–fork joint is rigid, and for $\hat{\Gamma}_{tf} \ll 1$, there is again a single effective degree of freedom due to the torque-free condition at the tail–fork joint. The small but non-zero swimming speeds measured for the robot even for the case of $\hat{\Gamma}_{tf} \ll 1$ and $\hat{\Gamma}_{tf} \gg 1$ (horizontal asymptotes in Fig. 3e) are attributed to effects of small but non-zero inertia, since $Re_{robot} \approx 0.2$,
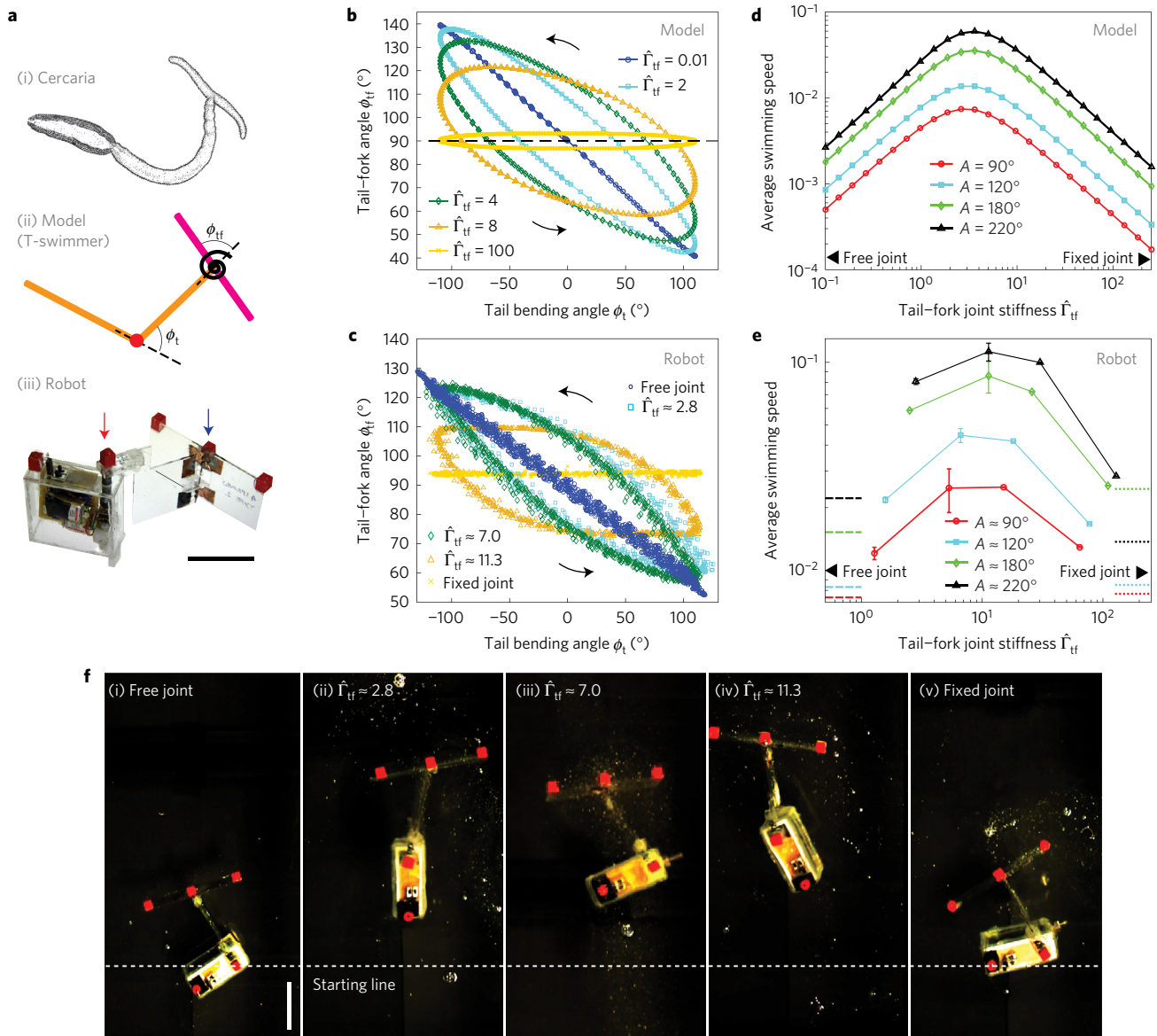
Figure 3 | Theoretical 'T-swimmer' and scaled-up robotic model for swimming S. mansoni cercariae. a, Schematics of (i) cercariae swimming tail-first and (ii) proposed 'T-swimmer' model. (iii) Photograph of a macroscale, self-propelled, 'T-swimmer' robot (Supplementary Methods) designed to swim in a high-viscosity fluid (corn syrup, viscosity $\mu \approx 8$ Pa s) chosen to be dynamically similar ($Re_{robot} \approx 0.2$) to swimming cercariae. The joint between the longitudinal links (red dot in (ii)) is active and actuated periodically with a given amplitude A and frequency f. The transverse joint is assumed to be a passive linear torsional spring (depicted as a black spiral) with stiffness Γ_{tf} to model the flexibility of the tail–fork joint in cercariae. The red and blue arrows in (iii) indicate the active and passive joints, respectively in the robot. Scale bar in (iii), 5 cm. **b,c**, Phase plots of the joint angles ϕ_{tf} and ϕ_t for a T-swimmer model (**b**) and robot (**c**) for a range of $\hat{\Gamma}_{tf}$, showing the non-reciprocal nature of the swimming cycle, where $\hat{\Gamma}_{tf}$ is Γ_{tf} normalized by the torque scale $\mu f l_c^3$. The arrows indicate the direction of phase trajectories. **d,e**, Plots of the average swimming speed (normalized by $f l_c$) for the T-swimmer model (**d**) and robot (**e**) as a function of $\hat{\Gamma}_{tf}$ for different actuation amplitudes A. Both the model (**d**) and robot (**e**) swim with the passive joint preceding the active joint, and the average swimming speed (normalized by $f l_c$) shows a single maximum at an $O(1)$ value of $\hat{\Gamma}_{tf}$, highlighting an optimal value of torsional stiffness for a given 'T-swimmer'. The horizontal lines in **e** indicate measured swimming speeds for a robot with a free joint (dashed lines) and fixed joint (dotted lines), respectively. These speeds are an order of magnitude smaller than the peak values. Error bars correspond to standard deviations over different experiments. **f**, Snapshots of final positions after 60 s of swimming for T-swimmer robots with a range of $\hat{\Gamma}_{tf}$ (i)–(v) and frequency maintained at ≈ 0.4 Hz. The white dashed line denotes the starting point of the robots. The free (i) and fixed joint (v) robots show relatively small displacements (Supplementary Movie 7). Scale bar in (i), 5 cm.

and in the $\hat{\Gamma}_{tf} \gg 1$ case, also due to the small bending degree of freedom that arises due to minute deflections in the material used to fabricate the robot. For both the T-swimmer and the robot, there is an intermediate value of torsional stiffness $\hat{\Gamma}_{tf}$ that optimizes the average swimming speed (Fig. 3d,e,f and Supplementary Movie 7). This happens due to resonant interaction between the driving timescale ($t_{forcing} = 1/f$) and the intrinsic

relaxation time of the torsional spring ($t_{relaxation} = \mu l_c^3/\Gamma_{tf}$)—that is, $1/f \sim \mu l_c^3/\Gamma_{tf}$.

As a next extension to the three-link T-swimmer, we added a fourth link to account for the thrust generated by the body in cercariae and also included the effects of gravity (Supplementary Section 2.2). This fourth link is attached longitudinally via a torsional spring to model the flexibility of the tail–body joint
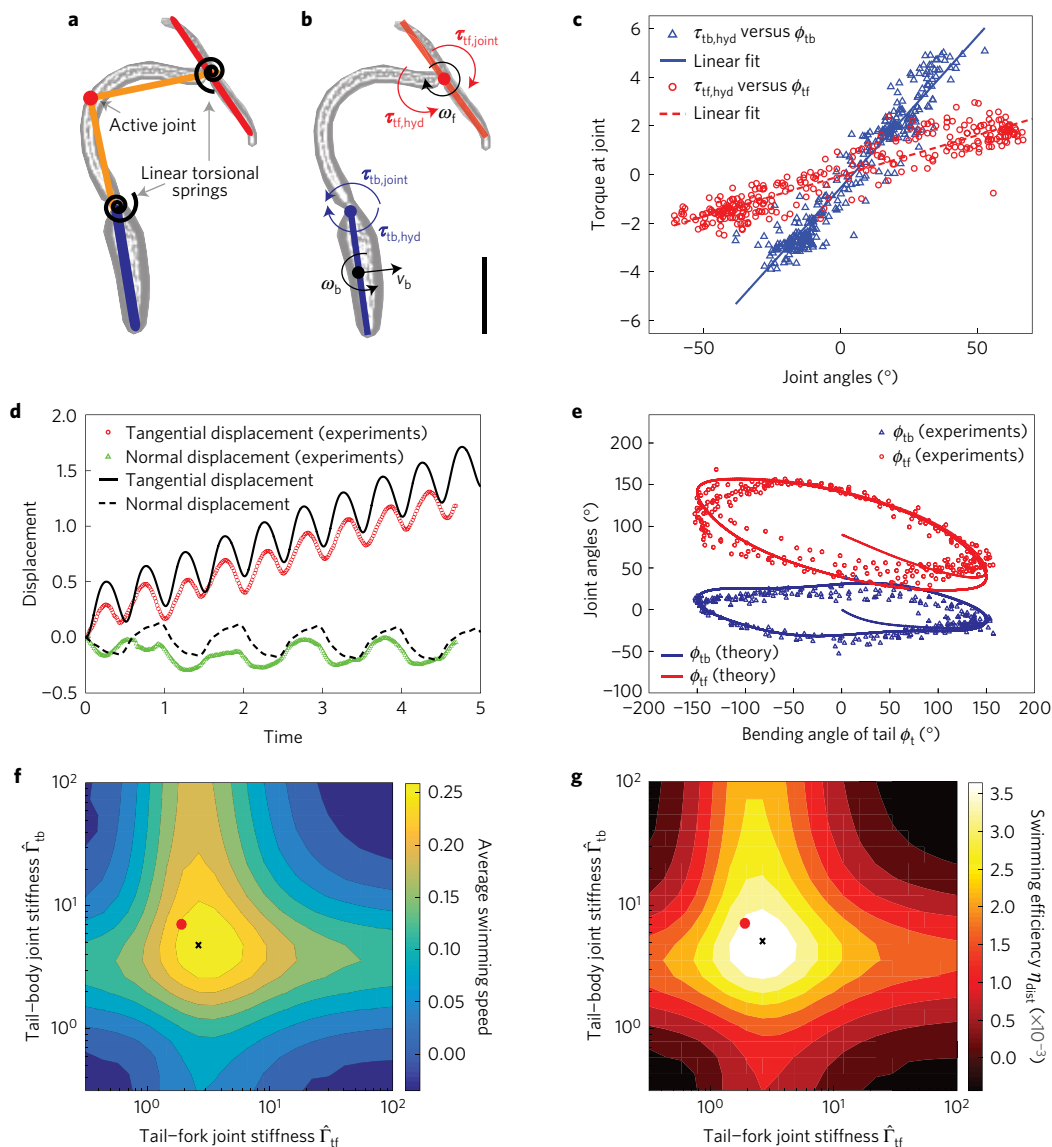
Figure 4 | Comparison between four-link 'T-swimmer' and swimming *S. mansoni* cercariae. a, Schematic of a four-link swimmer model overlaid on an image of a cercariae. The flexibility at the tail–fork and tail–body joints in cercariae is modelled via linear torsional springs, depicted as black spirals at the respective joints. **b**, Free body diagrams of the body and fork, showing translational and angular velocities and the resulting hydrodynamic torque about the respective joints. This torque is balanced instantaneously by the mechanical torques at the joints, thus allowing *in situ* means of estimating these torques (Supplementary Methods and Supplementary Section 2.3). Scale bar, 100 μm. **c**, Plot of the estimated torques (normalized by $\mu f l_c^3$) at the tail–body (blue triangles) and tail–fork (red circles) joints as a function of the corresponding joint angles ϕ_{tb} and ϕ_{tf} (over five swimming cycles). The slope of the respective linear fits (R-squared tail–body 0.7 and tail–fork 0.8) shown as solid blue and dashed red lines gives the joint stiffnesses ($\hat{\Gamma}_{tb}$ and $\hat{\Gamma}_{tf}$) in live, swimming cercariae. **d**, Time series plot of displacements (normalized by l_c) of the body along $\hat{s}$ and $\hat{n}$ for the four-link T-swimmer with estimated joint stiffnesses (black solid and dashed curves) compared with experimental measurements (red circles and green triangles). **e**, Phase plot between ϕ_{tb}, ϕ_{tf} and ϕ_t for the four-link T-swimmer, shown as blue and red lines, and for cercariae shown as blue triangles and red circles. **f,g**, Contour plots of average swimming speed (normalized by $f l_c$) (**f**) and swimming efficiency (**g**) as a function of the joint stiffnesses $\hat{\Gamma}_{tf}$ and $\hat{\Gamma}_{tb}$ show a single optimal point (black crosses). The red dots indicate the values estimated for cercariae, showing that they optimize their joint stiffnesses to swim efficiently.

(Fig. 4a). The resulting model can now be compared to experimental measurements on *S. mansoni* cercariae.

To make this comparison, we need the torsional spring stiffness of the two joints ($\hat{\Gamma}_{tb}$ and $\hat{\Gamma}_{tf}$) in a living (swimming) cercariae. We developed a novel *in situ* measurement using high-speed imaging data (Fig. 2) and hydrodynamic theory[25]. To do this, first we used slender-body-theory[19] to estimate the instantaneous torques at the two joints τ_{tf} and τ_{tb} from the translational and angular velocities of the fork and body (Fig. 4b and Supplementary Section 2.3). We then investigated the relationship between these torques and the corresponding joint angles ϕ_{tf} and ϕ_{tb} and found that they are

linearly correlated (Fig. 4c). This linearity implies that the two joints are indeed well approximated as linear torsional springs, serving as a posteriori verification of our T-swimmer model. Finally, we obtained the torsional spring stiffness of the two joints as the slopes of the linear fits.

By comparing our four-link T-swimmer with experiments on *S. mansoni* cercariae (Supplementary Movie 8), we find that the theoretical four-link T-swimmer indeed captures the swimming displacement per cycle (Fig. 4d) and the time evolution of the non-reciprocal joint angle kinematics very well (Fig. 4e). A crucial connection to disease transmission lies in the swimming efficiency

of this human parasite. Next, we estimate the cercarial swimming efficiency using our T-swimmer model. To measure how effectively cercariae can swim up the water column, we defined this efficiency as the ratio of average distance covered relative to the average viscous power dissipation in the fluid during a swimming cycle $\eta_{\text{dist}} = X_{\text{stroke}}/P_{\text{diss,stroke}}$ (Supplementary Section 3.1). By exploring a range of values in the $(\hat{\Gamma}_{\text{tf}}, \hat{\Gamma}_{\text{tb}})$ plane we find a single optimal point for both the swimming speed (Fig. 4f) and efficiency (Fig. 4g). Interestingly, we observed that the joint spring stiffnesses estimated for cercariae (red dots in Fig. 4f,g) lies close to this optimal peak. This suggests that cercariae maintain the stiffness of these two joints at the optimal range required for efficient swimming. This tuning may have resulted from strong evolutionary pressures on the parasite, since the host-seeking processes is energy constrained[5,6].

Our work points to an unusual elastohydrodynamic effect in cercarial swimming, where the tail provides the energy for propulsion but little thrust, while tail–body and tail–fork joints act as passive torsional springs providing most of the thrust. This passive control strategy is minimalistic in nature, where the only control lies in tuning the flexibility of the respective joints. Furthermore, cercariae are the first reported organisms to use both a longitudinal (the body) and transverse element (the fork)[14,26] to generate a net propulsion from bending waves propagating in opposite directions (due to the tail).

Since current mass drug administration strategies have significant limitations[27], mechanistically linking biophysics of human-seeking parasites such as *S. mansoni* to disease transmission in ecological field conditions could inspire a new paradigm of environmental control of this neglected tropical disease. The limited energy reserves of the cercarial stage of this parasite may be its Achilles heel. Being of a higher density than water, simply targeting the swimming motility could impair the parasites ability to aggregate near the air–water interface, thereby reducing transmission rates. Towards this, our study of the swimming mechanics has given the first quantitative estimate of the swimming efficiency, and allows an understanding of how perturbations to various parameters affect the motility of cercariae.

Data availability. The data that support the plots within this paper and other findings of this study are available from the corresponding author upon request.

References

1. Haas, W. Physiological analysis of cercarial behavior. *Physiol. Anal. Cercarial Behav.* **78,** 243–255 (1992).
2. Haas, W. Parasitic worms: strategies of host finding, recognition and invasion. *Zoology* **106,** 349–364 (2003).
3. Hotez, P. J. & Kamath, A. Neglected tropical diseases in sub-Saharan Africa: review of their prevalence, distribution, and disease burden. *PLoS Negl. Trop. Dis.* **3,** e412 (2009).
4. Hotez, P. J. & Fenwick, A. Schistosomiasis in Africa: an emerging tragedy in our new global health decade. *PLoS Negl. Trop. Dis.* **3,** e485 (2009).
5. Lawson, J. R. & Wilson, R. The survival of the cercariae of *Schistosoma mansoni* in relation to water temperature and glycogen utilization. *Parasitology* **81,** 337–348 (1980).
6. Whitfield, P. J., Bartlett, A., Khammo, N. & Clothier, R. H. Age-dependent survival and infectivity of *Schistosoma mansoni* cercariae. *Parasitology* **127,** 29–35 (2003).
7. Purcell, E. M. Life at low Reynolds number. *Am. J. Phys.* **45,** 3–11 (1977).
8. Haas, W., Beran, B. & Loy, C. Selection of the host's habitat by cercariae: from laboratory experiments to the field. *J. Parasitol.* **94,** 1233–1238 (2008).
9. Combes, C., Fournier, A., Moné, H. & Théron, A. Behaviours in trematode cercariae that enhance parasite transmission: patterns and processes. *Parasitology* **109,** S3 (1994).
10. Graefe, G., Hohorst, W. & Dräger, H. Forked tail of the cercaria of *Schistosoma mansonia* rowing device. *Nature* **215,** 207–208 (1967).
11. Nuttman, C. *The Structure and Behaviour of the Cercaria of Schistosoma Mansoni* PhD thesis, Univ. York (1975).
12. Berg, H. C. *Random Walks in Biology* (Princeton Univ. Press, 1993).
13. Lauga, E. & Powers, T. R. The hydrodynamics of swimming microorganisms. *Rep. Prog. Phys.* **72,** 96601 (2009).
14. Subramanian, G. & Nott, P. R. The fluid dynamics of swimming microorganisms and cells. *J. Indian Inst. Sci.* **91,** 283–314 (2012).
15. Bundy, D. Swimming behaviour of the cercaria of *Transversotrema patialense*. *Parasitology* **82,** 319–334 (1981).
16. Haas, W., Haeberlein, S., Behring, S. & Zoppelli, E. *Schistosoma mansoni*: human skin ceramides are a chemical cue for host recognition of cercariae. *Exp. Parasitol.* **120,** 94–97 (2008).
17. Brachs, S. & Haas, W. Swimming behaviour of *Schistosoma mansoni* cercariae: responses to irradiance changes and skin attractants. *Parasitol. Res.* **102,** 685–690 (2008).
18. Haas, W. *et al*. Recognition and invasion of human skin by *Schistosoma mansoni* cercariae: the key-role of L-arginine. *Parasitology* **124,** 153–167 (2002).
19. Leal, L. G. *Advanced Transport Phenomena: Fluid Mechanics and Convective Transport Processes* Vol. 7 (Cambridge Univ. Press, 2007).
20. Wiggins, C. H. & Goldstein, R. E. Flexive and propulsive dynamics of elastica at low Reynolds number. *Phys. Rev. Lett.* **80,** 3879–3882 (1998).
21. Cox, R. G. The motion of long slender bodies in a viscous fluid part 1. General theory. *J. Fluid Mech.* **44,** 791–810 (1970).
22. Reger, J. F. Studies on the fine structure of cercarial tail muscle of *Schistosoma* sp. (Trematoda). *J. Ultrastruct. Res.* **57,** 77–86 (1976).
23. Nuttman, C. The fine structure and organization of the tail musculature of the cercaria of *Schistosoma mansoni*. *Parasitology* **68,** 147–154 (1974).
24. Passov, E. & Or, Y. Dynamics of Purcell's three-link microswimmer with a passive elastic tail. *Eur. Phys. J. E* **35,** 1–9 (2012).
25. Friedrich, B., Riedel-Kruse, I., Howard, J. & Jülicher, F. High-precision tracking of sperm swimming fine structure provides strong test of resistive force theory. *J. Exp. Biol.* **213,** 1226–1234 (2010).
26. Brennen, C. Locomotion of flagellates with mastigonemes. *J. Mechanochem. Cell Motil.* **3,** 207–217 (1975).
27. Cioli, D., Pica-Mattoccia, L., Basso, A. & Guidi, A. Schistosomiasis control: praziquantel forever? *Mol. Biochem. Parasitol.* **195,** 23–29 (2014).

Author contributions

D.K. and M.P. designed the research. D.K., G.K. and M.P. performed experiments. G.K. and D.K. performed image analysis. D.K. and A.B. performed the scaled-up robotic experiments and D.K. performed numerical simulations. D.K., G.K. and M.P. analysed the results and wrote the manuscript.

Additional information

Supplementary information is available in the online version of the paper. Reprints and permissions information is available online at www.nature.com/reprints. Correspondence and requests for materials should be addressed to M.P.

Competing financial interests

The authors declare no competing financial interests.